Nanoscale

Accepted Manuscript

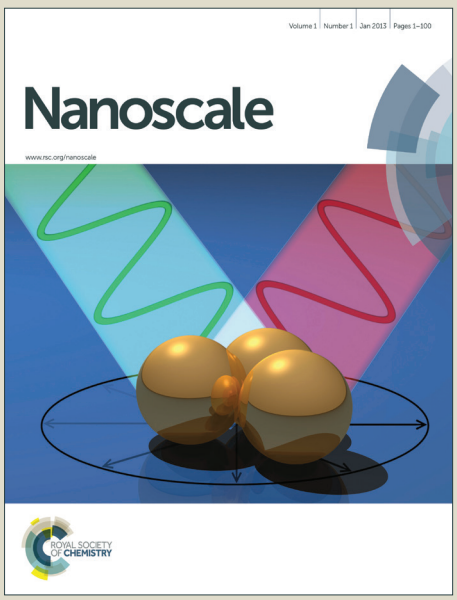

ROYAL SOCIETY OF CHEMISTRY

www.rsc.org/nanoscale

Nanoscale

RSCPublishing

ARTICLE

Ultrathin InAs Nanowire Growth by Spontaneous Au Nanoparticle Spreading on Indium-Rich Surfaces

Kyooho Jung, Parsian K. Mohseni, and Xiuling Li*

Ultrathin InAs nanowires (NWs) can enable true one-dimensional electronics. We report a growth phenomenon where a bimodal size distribution (~α nm and ~5 nm in diameter) of InAs NWs can be formed from gold (Au) nanoparticles of a single size, α (α = 50 – 250 nm). We determine that ultrathin InAs NW growth is seeded by ultra-small Au nanoparticles shed from the large Au seeds upon indium (In) introduction into the growth system and formed prior to the supersaturation of In in Au. The Au spreading phenomenon is explained by the balancing of Gibbs free energy lowering from In-Au mixing and surface tension increase. Ultrathin InAs NWs formed in this way exhibit a perfect wurtzite structure with no stacking faults. We have observed InAs NWs down to ~2 nm diameter using our growth method. Passivating the ultrathin InAs NWs with an AlAs shell, subsequently oxidized in air, results in physical deformation of the InAs core, demonstrating the mechanical pliability of these ultrathin NWs.

1. Introduction

For the past several decades, Si CMOS field effect transistors (FETs) have scaled continuously according to Moore's Law, enabling the modern information age, and are expected to reach the sub-10 nm node within the next few years[1]. In the sub-10 nm regime, short channel effects are even more pronounced, which will limit the performance of nanometer-scale transistors[2,3]. Various designs have been suggested to overcome the short channel effect such as the finFET, double gate, surround gate, and ultrathin body transistors[4-7]. These designs require body thicknesses equal to or smaller than the gate length to effectively suppress the short channel effects[8], which means that in the sub-10nm regime, body thickness of below 10 nm will be required.

In parallel to the aggressive scaling of Si CMOS, III-V semiconductor materials have been positioned to be one of the top candidates for the beyond-Si roadmap[1]. Low bandgap III-V semiconductors such as InAs, with their high electron mobility and high electron injection velocity, are especially promising. In addition, transistors that employ one-dimensional ballistic transport nanowire (NW) channels, achievable only when the diameter is extremely small, can operate in the quantum capacitance limit (QCL) to achieve high performance and high linearity RF operation[9,10].

Critical to small III-V NWs, etching and implantation should be avoided to minimize surface damage, thus bottom-up growth is preferred. Several theoretical studies predicted a Gibbs-Thomson effect limited critical nanowire diameter by the metal-catalyzed vapor-liquid-solid (VLS) mechanism[11,12]. This is because of the highly elevated chemical potential for small catalyst particles, which is obviously is a function of growth parameters including temperature, pressure, and growth rate. Although the growth of sub-5 nm nanowires of In_2O_3, InSb, and GaAs have been demonstrated[13,14,15], to our knowledge, there is no systematic experimental study on how to overcome the diameter limit dictated by the Gibbs Thompson effect for VLS nanowires.

Here, we report the growth and characterization of ultrathin InAs NWs, with diameters as low as ~2 nm and free of crystal stacking faults, using a unique Au nanoparticle spreading phenomenon during growth by metalorganic chemical vapor deposition (MOCVD). Detailed experimental analysis of the growth method is carried out to determine the conditions under which the Au spreading behavior occurs as well as methods for suppression of atomic Au diffusion along the growth substrate. Furthermore, AlAs and GaAs/AlAs shells have been grown over such ultrathin InAs NWs to examine the core-shell interface quality and the core integrity near the critical diameter. This unique growth mode yields high quality ultrathin InAs NWs that are suitable for the fabrication of devices with potential applications in high speed and low power high linearity nano-electronics[16,17].

2. Experimental section

InAs NWs were grown by MOCVD using an Aixtron 200/4 reactor via the Au-assisted vapor-liquid-solid (VLS) mechanism. Prior to growth, InAs (110) and (100) substrates were cleaned in acetone, IPA, DI water, and were etched in HCl/H_2O (1:10) for removal of the native oxide layer. Au colloidal particles (BBInternational, 50 nm - 250 nm in diameter) were dispersed onto the wafer surface using pipettes and dried under N_2 flows. As-prepared samples were immediately loaded into the MOCVD chamber for InAs NW growths. Poly-l-lysine (Ted Pella) was used in all of our studies to increase the Au particle density and distribution uniformity. Control experiments performed without the use of poly-l-lysine gave the same results, except for the density of the large Au seeds showing

that the poly-l-lysine does not affect the ultra-thin nanowire growth under the conditions explored. Trimethyl-indium (TMIn), trimethyl-gallium (TMGa), and arsine (AsH_3) were used as In, Ga, and As precursors, respectively, with hydrogen (H_2) as the carrier gas. The NWs were grown between 420˚C and 450˚C, and depending on the temperature and substrate orientations, V/III ratios in the range of 9.8 to 16.3 were used for ultrathin InAs NW growth. The NWs were characterized using a Hitachi S-4800 scanning electron microscope (SEM), a JEOL 2010 LaB_6 high-resolution transmission electron microscope (HRTEM), and a JEOL 2010F EF-FEG scanning transmission electron microscope (STEM). Energy dispersive X-ray spectrometry (EDXS) analysis was performed on NWs dispersed on Cu TEM grids in STEM mode.

3. Results and discussion

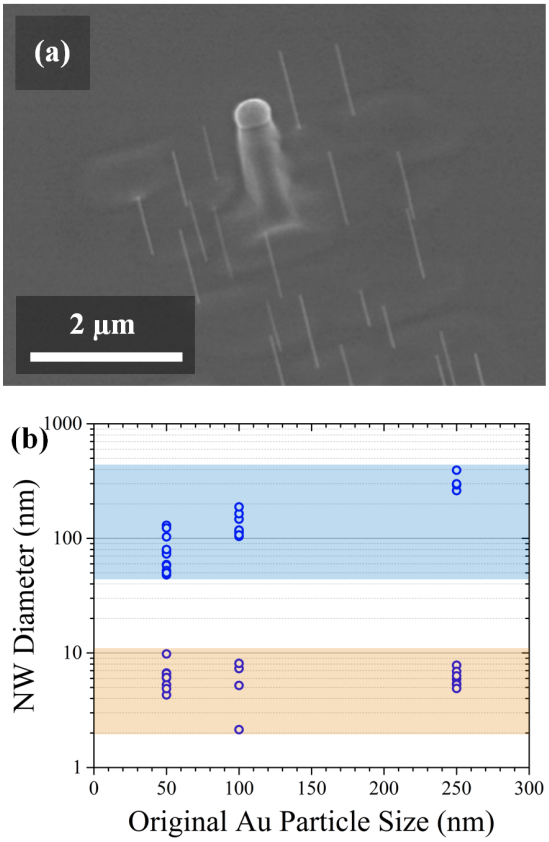

Figure 1. Bimodal size distribution. (a) SEM image of InAs NWs grown at 450˚C with nominal V/III = 10.9 on an InAs (100) substrate using 250 nm Au colloidal particles. (b) Plot showing the correlation between the Au particle size (x-axis) and produced NW size (y-axis) on a logarithmic scale. A bimodal distribution of the NW size can be seen for all Au nanoparticle sizes, with the large ones (blue-highlighted region) close to the original Au particle size, and the small size group (orange-highlighted region) all falling below 10 nm, irrespective of the starting seed size.

Figure 1(a) shows an SEM image of InAs NWs grown at 450˚C on an InAs (100) substrate using 250 nm Au colloids and nominal V/III ratio of 10.9. As can be seen, the NWs exhibit a bimodal size distribution where ultrathin and larger InAs NWs coexist. The diameters of the larger NWs match the size of the Au colloids used, while those of the smaller NWs typically range between 4 to 8 nm, which is 2 orders of magnitude smaller than the size of the Au colloids initially dispersed onto the growth substrates. The bimodal growth can be observed for various Au particle sizes and also on InAs (110) substrates (Figure S1, Supplementary Information). Under the specified growth conditions, on InAs (100) substrates, larger NWs always show planar growth similar to GaAs NWs previously reported in the literature[18,19], whereas the ultrathin NWs tend to grow off the substrate plane in one of the two equivalent <111>B directions, based on the ~35° growth angle of NWs with respect to the substrate. A bimodal NW size distribution has also been observed on InAs (110) substrates (Figure S1c, Supplementary Information). However, in contrast to (100) substrates, both the large and ultrathin NWs grow out-of-plane under the specified growth condition; and only in the singly available [111]B direction, similar to other III-V nanowires reported in the literatures[20,21]. Under the optimized ultrathin InAs growth condition which does not show any noticeable tapering, the ultrathin InAs NWs have a growth rate of ~100 nm/min. Under the growth parameter space explored, these ultrathin NWs can be grown up to 3 µm in length while maintaining uniform ~5 nm diameters, corresponding to an aspect ratio of 600:1 (Figure S2, Supplementary Information). Beyond that length, noticeable tapering through base broadening is observed and the

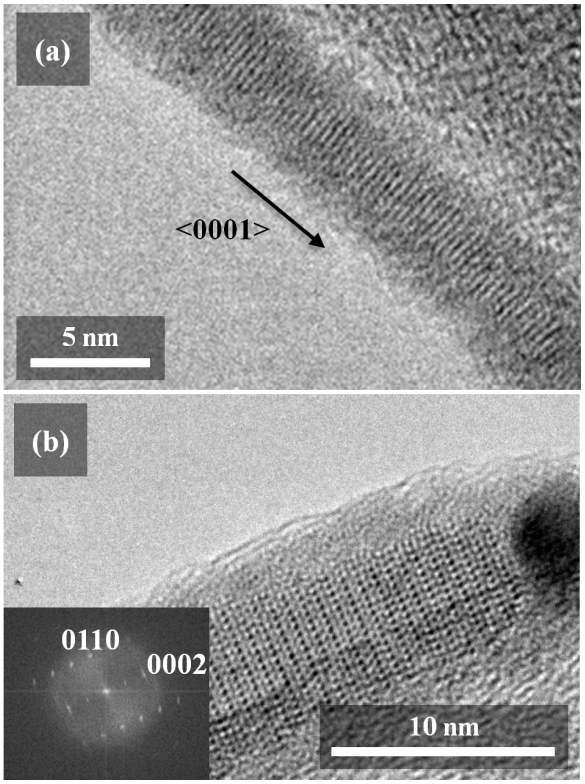

Figure 2. HRTEM image of ultrathin InAs NWs. (a) A 2.14 nm diameter InAs NW with <0001> growth direction, showing a WZ structure without stacking faults, and (b) a 5.5 nm diameter InAs NW showing WZ crystal structure without stacking faults (the NW was oriented along the $< 2\bar{1}\bar{1}0 >$ zone axis; Inset shows a corresponding FFT pattern).

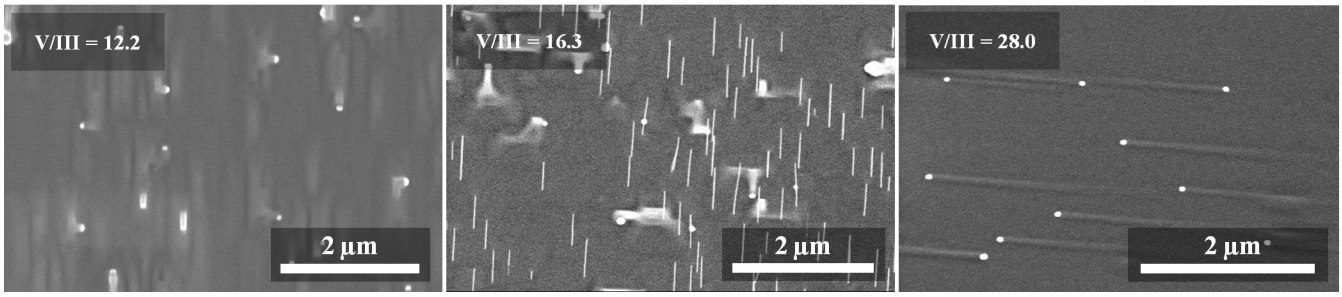

Figure 3. Effect of V/III ratio on the ultrathin InAs NW growth. All of the samples were grown at 420˚C on InAs (100) wafers for 20 minutes using 50 nm Au colloids. At V/III=12.2, no ultrathin growth was observed. At V/III=16.3, ultrathin InAs NWs grow. At V/III = 28, no ultrathin NW could be observed and only the planar NWs that grew out of the original Au particles could be seen.

diameter of the ultrathin NWs also become larger, presumably due to direct growth on the NW sidewalls. The ultrathin InAs NWs can be grown across the entire sample area except near the substrate edge (~1 mm from the edge), where the NWs are longer and thicker. Such enhanced lateral and vertical growth rates in the peripheral regions can be attributed to the so called "edge-effect", commonly observed in NW growths using MOCVD[22]. Interestingly, the ultrathin InAs NWs grow only within certain proximity to the original large Au nanoparticle locations on the substrates. This can be clearly seen when the density of the Au nanoparticles is low for growths from 50 nm to 250 nm Au nanoparticles (Figure S3, Supplementary Information).

The proximity radius appears to increase with increasing size of the original Au nanoparticle deposited onto the substrates. For example, the distance of the furthest ultrathin NW to the original Au nanoparticles is ~3 µm for 250 nm Au nanoparticles and ~1.5 µm for 50 nm Au nanoparticles. This proximity effect indicates that ultrathin InAs NW growth could be originated from the larger Au particles due to splitting and diffusion.

HRTEM analysis of the ultrathin InAs NWs indicates that the crystal structure is hexagonal wurtzite and that growth ensues along the [0001] direction. The stacking fault densities vary depending on the growth conditions and substrates used. Figure 2a shows the atomic structure of one of the smallest InAs NWs grown at 450 ˚C on a (110) InAs substrate that originated from 50 nm Au nanoparticles. The NW diameter is measured to be roughly 2 nm. Under this growth condition, all of the NWs are nearly stacking fault-free. Figure 2(b) shows the atomic structure of an InAs NWs with a diameter of ~5.5 nm grown at 420 ˚C on a (100) InAs substrate. The ~1.2 nm thick native oxide layer can also be seen clearly in this image. The lattice constant in the axial direction is measured to be 6.99 Å, which matches previously reported experimental values for wurtzite-phase InAs NWs[23]. The NW diameter is quite uniform with only ~1 nm difference from the base to the tip, at this low growth temperature (420 ˚C), where vapor-solid deposition on the NW sidewalls is suppressed. Compared to stacking fault-free ultrathin NWs grown at 450˚C, those grown at 420 ˚C show stacking fault densities of ~20 μm^{-1}, on average.

Importantly, 4-5 nm size particles can be observed at the tip of every ultrathin NW, although much larger Au particles (50 nm ~ 250 nm) were deposited onto the growth substrate before growth. EDXS composition analysis (Figure S4, Supplementary Information) reveals that the NW tips are composed purely of Au, confirming the VLS growth mechanism. Furthermore, we emphasize that prior to the onset of NW growth (after Au colloid dispersal), no evidence of a bimodal distribution of Au nanoparticles has been observed. As no alternative source for the presence of correspondingly small Au nanoparticle seeds has been identified, we expect that they can only result from splitting from the larger, originally deposited Au particles and that subsequent atomic diffusion occurs either before growth or at the growth temperature.

A finite V/III ratio window exists for the growth of InAs NWs with a bimodal size distribution. Beyond a fixed V/III ratio range, no ultrathin NWs can be observed, and within the growth window, the V/III ratio can be varied to obtain either ultrathin InAs NWs with uniform diameters or tapered morphologies. Shown in Figure 3 are SEM images of a series of samples grown at 420 ˚C on InAs (100) wafers for 20 minutes using 50 nm Au colloids at different V/III ratios. At V/III = 12.2, no ultrathin NW growth is observed. At V/III = 16.3, ultrathin InAs NWs can be clearly seen. At V/III = 28, no ultrathin NWs are observed and only planar NWs, corresponding to the size of the original Au particles, are found. Between V/III of 12.2 and 28, the ultrathin NWs gradually become more tapered with higher V/III ratios in which the tip size is ~5 nm but the base of the NWs reach up to over 100 nm in diameter. On the other hand, to obtain uniform diameter ultrathin InAs NWs on InAs (100) wafers at 450˚C, a nominal V/III ratio of ~ 11.5 is optimal, in contrast to a V/III ratio of 16.3, which is required at 420˚C. Considering the increased AsH_3 cracking rate at higher temperatures, the effective V/III ratio might be similar at all temperatures.

A model for Au atom diffusion for the origin of the bimodal size distribution in the growth of NWs had previously been reported by Dailey and Drucker, in which silicon and germanium NWs of dual diameter sizes had been observed[24]. The authors attributed their observation to the monolayer thick Au/Si(111) films that were formed between three-dimensional (3-D) Au islands prior to NW growth, originating during Au film deposition. The authors claimed that upon hydrogen introduction into the growth chamber, the monolayer Au films between the Au islands de-wet the surface to form ~15 nm Au particles, which then led to smaller NW growth along with the large NWs seeded from the Au islands. In our case, the growth was carried out using Au colloids and no such Au film was present between the colloidal particles to form the second mode of the size distribution. In addition, no bimodal size distribution has been observed for Au-assisted GaAs (instead of InAs) NW growth in the same reactor using the same Au colloid seeds under various conditions explored, indicating that the ultra-small Au seeds are not formed without the presence of indium.

Hertog et al. and Madras et al. have previously reported on the phenomenon of Au surface diffusion occurring during silicon

NW growth to form smaller Au particles[25,26]. Madras observed via in-situ TEM that, under certain conditions, Au can diffuse to the NW sidewalls in the form of AuSi and can separate from the liquid layer to form 3-5 nm Au particles upon cooling down. In our case, however, ultrathin InAs NWs grow out of smaller Au particles based on EDXS analysis in TEM, which is clear evidence that the smaller Au particle formation occurs not during cool-down but, rather, prior to ultrathin NW growth. Combined with the Au-assisted GaAs NW control experiment mentioned above, we hypothesize that the onset of Au diffusion forming the ultra-small particles that seed ultrathin NW growth results from the combination of InAs growth onset, Au spreading, and the appropriate growth condition.

To further examine at which point the ultra-small Au particles are formed, two sets of experiments were carried out. First, we held the InAs substrates with 250 nm Au particles deposited at the growth temperature under 200 mbar under H_2 and AsH_3 flows for 15 minutes prior to the initiation of the InAs NW growth. If it is energetically favorable for the large Au particles to spread out and form smaller Au particles before TMIn introduction, then this longer incubation time should lead to the ultrathin InAs NWs forming further away from the 250 nm Au particles or lead to higher ultrathin InAs NW density. Indeed, we have determined that holding the temperature does not change the maximum ultrathin InAs NW growth distance from the larger, originally deposited seeds or their density, as compared to those without the temperature hold (Figure S5, Supplementary Information). Second, there is a possibility that the Au atoms diffuse out of the larger Au particles during the NW growth as previously observed by Hannon et al.[27]. To examine validity of this case in relation to the current study, we extended the NW growth time by a factor of 10 to establish whether there is a size reduction in the larger Au particles. The growth conditions were the same as the NWs in Figure S1(c), except for the increased growth time. We found that there is no size reduction of the Au particles during the NW growth (Figure S6, Supplementary Information). Thus, we conclude that the formation of the ultra-small (~5 nm) Au particles occurs after the TMIn introduction into the chamber, but stops once the larger Au particles supersaturate and nucleate to form NWs. The fact that neither the ultrathin InAs NWs nor the sub-10 nm Au particles could be observed on the sidewall of the larger NWs (Figure S7, Supplementary Information) further supports our claim that Au atom diffusion is inhibited once the Au catalysts are fully saturated with In.

From the experimental observations above, we can establish that two conditions must be satisfied in order for the Au atoms to spread out of the larger Au particles to form smaller ones: (i) relatively high level of TMIn must be introduced into the system (i.e. low V/III ratio), and (ii) Au catalysts should not be fully saturated with In. Condition (ii) implies that the Gibbs energy of Au-In mixing affects the Au atom diffusion process. Gibbs energy of mixing in the binary Au-In system has been reported by several groups. It was shown that the normalized Gibbs free energy of mixing (GM/RT), under the condition similar to our NW growth system, has a minimum value of almost -3 at 45.5% In composition[28], which indicates that the alloying of Au and In lowers the energy of the catalyst significantly. Also, the Au and In alloy is known to show extremely rapid inter-diffusion[29]. Combining the factors noted above, we believe that the spreading of Au particles occurs via the following process: The introduction of high TMIn flow into the growth chamber provides an indium-rich environment on the InAs surface. Au nanoparticles start to form alloys with In, thus, forming Au-In droplets. However, during the incubation period, Gibbs free energy lowering from the intermixing of Au and In, combined with the local Au concentration gradient, acts as a driving force for Au atom diffusion into the In-rich surface, forming an In-rich, Au-In film in the vicinity of the dispersed Au nanoparticles. The thickness of the Au-In thin film is estimated to be on the order of ~ 2 -3 Å[25,26,30]. Due to the rapid inter-diffusion process between Au and In, Au-In film can propagate as far as several μm from the original Au seeds. Au atoms then continue to diffuse out from the catalyst nanoparticles as long as the energy lowering from the Au-In alloying and the diffusion driving force from the Au concentration gradient is larger than the surface tension increase from the nanoparticle curvature decrease. Thus, when the Au catalyst reaches a certain In saturation level, the diffusion of the Au atoms will stop. Au atoms that have diffused out will seed the growth of ultrathin NWs once they reach the critical size to overcome the Gibbs-Thomson effect. Although it is currently unclear, there may be several justifications for ultrathin InAs NWs not appearing when the V/III ratio is below the critical value. First, Au atoms may not have diffused out due to fast supersaturation of the Au catalyst under high TMIn flow. This, however, is unlikely because even at the lower V/III limit of the bimodal growth condition, the ultrathin NWs appear several microns away from the original Au catalysts. Second, the Au atoms may have diffused out, but due to the large Gibbs-Thomson effect on the smaller Au nanoparticles, the NWs may not grow out of the smaller Au nanoparticles and, therefore, become buried in the InAs films grown above. The surface morphology of the samples grown below the critical V/III limit for bimodal growth condition for a brief growth period (<1 min) shows small etched pits near the original Au catalysts dispersed onto the substrates (Figure S8). These small pits are akin to Au etched surfaces often observed during the early stages

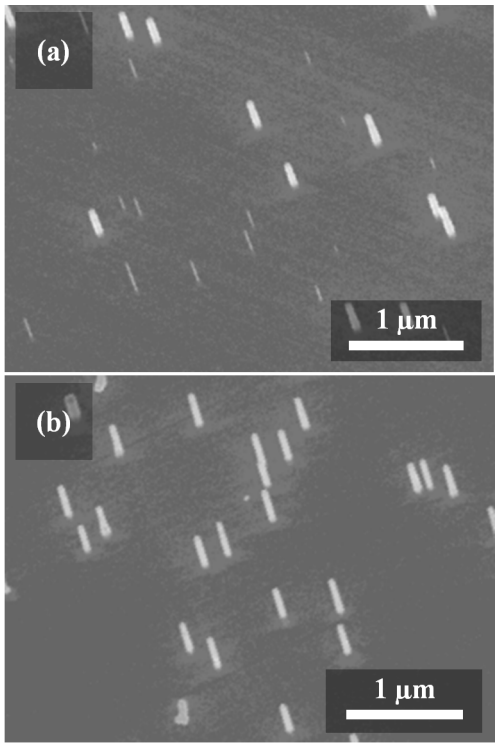

Figure 4. (a) InAs NWs grown on InAs(110) substrates under typical bimodal growth condition (450 ˚C, V/III = 9.8) for 3 minutes. (b) InAs NWs grown using high V/III ratio (V/III = 28) incubation time of 10 minutes followed by growth under typical bimodal NW condition for 3 minutes. Ultrathin InAs NWs cannot be observed.

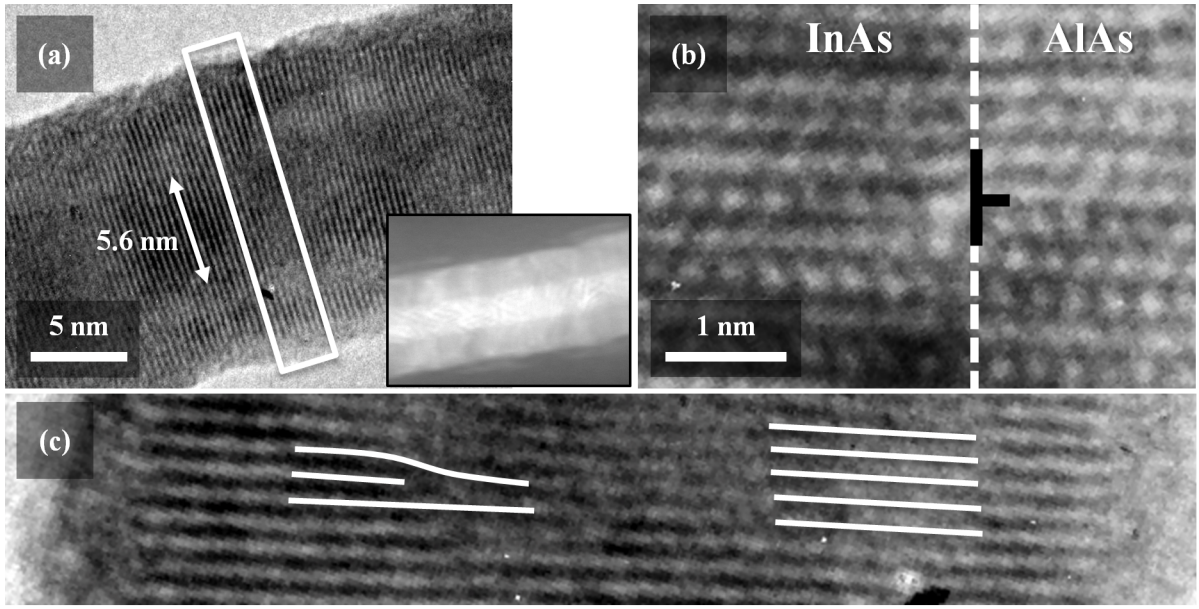

Figure 5. (a) HRTEM image of the NWs with 5.6 nm InAs core and 3.7 nm AlAs/GaAs shell. The inset shows an HAADF image of the NW with clear contrast between the core and the shell. (b) High resolution image showing the interface between the InAs and AlAs. The edge dislocation induces local zinc blende-type stacking in the shell region. (c) Magnified view of the yellow square region in (a) showing edge dislocation at the InAs/AlAs interface. Notice that the edge dislocation is observed only on one side of the NW.

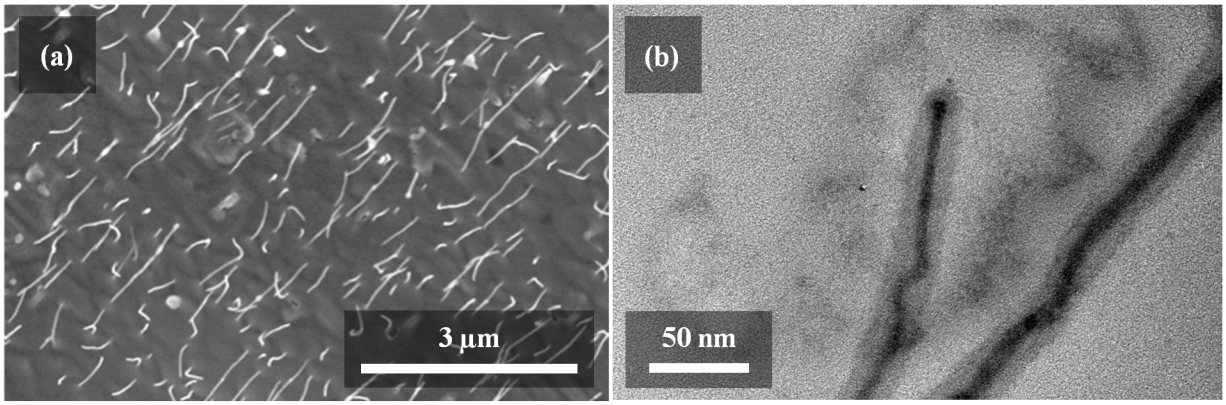

Figure 6. (a) SEM and (b) HRTEM images of physically deformed ultrathin InAs NWs passivated with AlAs shells, which were subsequently oxidized when brought into atmosphere. The oxide thickness is measured to be ~ 8 nm and the InAs core diameters typically range between 4 – 8 nm.

of NW growth or when there is little or no source flow at a high temperature[31]. This supports the second hypothesis and shows that even below the critical V/III ratio for bimodal growth, Au atom diffusion occurs.

To further support our Au atom spreading mechanism, we have carried out a two-step InAs NW growth in which NWs were grown first under high V/III ratio and then at a typical bimodal growth condition. The purpose of the first growth step under high V/III ratio is to prevent Au atom diffusion during the incubation period of the Au catalysts. Figure 4 shows comparison of InAs NWs grown on InAs (110) substrates using 50 nm Au nanoparticles with and without this high V/III ratio incubation period. The InAs NWs in Figure 4(a) have been grown under the typical bimodal growth condition (450 ˚C, V/III = 9.8) for 3 minutes, whereas in Figure 4(b), the sample has been held under V/III ratio of 28 for 10 minutes, followed by 3 minutes of growth under the same condition as sample in Figure 4(a). Indeed, the high V/III ratio incubation period has effectively inhibited the diffusion of the Au atoms on the wafer surface.

Our Au atom diffusion mechanism can be used to explain several observations mentioned previously. First, the fact that ultrathin InAs NWs could be observed further from the larger Au nanoparticles can be explained from the fact that the incubation period for the larger Au nanoparticles are longer, and so the Au atoms diffuse further. Second, the absence of ultrathin InAs NWs above a certain critical V/III ratio can be explained by the fact that an In-rich surface is required in order for the Au atoms to diffuse out. Third, the absence of small Au particles on the NW sidewalls grown out of original Au seeds can be attributed to the termination of the Au atom diffusion after supersaturation and nucleation of the larger NWs.

Surface passivation of the InAs NWs is critical for optical and electronic devices. Two types of shells are explored here on the ultrathin InAs NWs which are AlAs and AlAs/GaAs. Passivation with the AlAs layer was done under the same temperature as the InAs core growth but with a higher V/III ratio of 75 to enhance radial growth and suppress axial growth. An atomically abrupt and defect-free interface between the core and the shell is required to remove surface states and reduce carrier leakage for the core-shell radial heterojunction. Because AlAs becomes oxidized into an amorphous layer when brought into air, abrupt crystalline interfaces cannot be assured. Therefore, we grew an additional GaAs layer following the AlAs shell, which was also grown under the same temperature as the core but with a V/III ratio of 170. Figure 5 shows TEM images of an InAs/(AlAs/GaAs) core/multishell NW with thicknesses of 5nm/(4nm/2nm), respectively. With GaAs protection, no amorphous shell was observed beyond the InAs core. Because the GaAs outer shell is very thin (< 2 nm), the thickness-contrast cancels the Z-contrast, such that no clear difference between AlAs and GaAs can be seen in bright-field TEM or high-angle annular dark-field (HAADF) STEM images. However, the fact that AlAs has maintained its crystallinity shows that the GaAs does exist outside AlAs layer, preventing AlAs from oxidation. On the other hand, a clear contrast can be seen between the InAs core and the AlAs layer. Slight bending of the NW can also be seen in the inset of Figure 5(a), presumably as a result of the incomplete strain relaxation in the shell. Raychaudhuri et al. have predicted that two types of edge dislocations can be formed in core-shell heterostructured NWs in which edge dislocations form with a Burger's vector pointing either toward the axial direction or toward tangential direction to the interface between the core and the shell[32,33]. As the theory predicts, edge dislocations, which surround the core, can be observed in the HRTEM images shown in Figure 5. However, most of the edge dislocations' positions do not appear on both sides of the NW, as shown in Figure 5(c), which implies that the edge dislocations do not completely surround the NW's circumference in a loop-form as was observed by Popovitz-Biro et al. for InAs/GaAs core/shell NWs[34]. Such 'non-matching' dislocations have been reported recently in the case of Ge/Si core/shell NWs, whereas perfect dislocations surround the Si NW core segments in a slanted loop fashion[35]. Our NWs, however, have a wurtzite crystal structures for both the core and the shell, and in the wurtzite system, slip planes are either parallel or perpendicular to the [0001] direction, meaning that the slanted dislocations are extremely unlikely to exist. Lattice resolved image of the InAs/AlAs interface with an edge dislocation shows that the dislocation induces local zinc-blende type stacking, implying that the edge dislocation is indeed of the Frank-type partial dislocation. Further study will be needed to completely understand the non-matching dislocations in our core/shell NWs. The edge dislocations occur approximately every 20 atomic planes, which corresponds to ~5% relaxation in the shell along the axial direction. This value is much lower than the mismatch value between InAs and AlAs showing that the shell is only partially relaxed. Although theories predict that critical diameter of the core exists, below which no dislocation forms[33], with the core-shell dimension (5nm/6nm) and composition mismatch (~ 7%) in this study, the core-multishell structure is clearly not coherent.

Figure 6 shows SEM and TEM images of 4 nm thick AlAs-passivated ultrathin InAs NWs, without the GaAs cap, after being exposed to air. The shell appears to be fully oxidized with a measured thickness of 8 nm. It can be seen that the core has been mechanically deformed, yielding twisted NW morphologies. It is evident that the formation of the amorphous oxide shell, with its expanded volum, has imposed stress on the single crystal InAs core. In this case, the NW core is thin enough such that it can share the strain by twisting in a "zigzagging" manner, demonstrating its mechanical flexibility. In contrast, for planar thin films, strain relaxation occurs only in the thin films with negligible deformation in the body of the substrate due to the large difference in thickness. Note that the core diameter as well as the shell thickness is uniform throughout the entire NW and, thus, the deformation is not a result of anisotropic strain stemming from an uneven passivation layer. Such twisted, zigzagging NWs have not been previously realized through standard in-situ growth methods, as the NW shell thicknesses are typically much thinner than the core diameter.

4. Conclusions

We have reported a growth method to produce ultrathin InAs NWs that can enable unique electronic devices, such as those that require true one-dimensional density of states to operate in the QCL. The ultrathin InAs NWs formed this way exhibit a perfect wurtzite crystal structure. We have found that the In-rich environment is required for the Au nanoparticle splitting and spreading. A mechanism that involves the balancing of Gibbs free energy lowering from In-Au mixing and increasing surface tension from particle size reduction is proposed to explain the Au spreading phenomenon, and verified by control experiments using various V/III ratios and incubation periods. Abrupt InAs/AlAs core/shell heterointerfaces have been demonstrated. Although much less defective than is expected in planar epitaxial thin films, loop edge dislocations exist even with ultrathin cores of ~5 nm and thin shells of ~3 nm. Passivating the ultrathin InAs NWs with an AlAs shell that is subsequently converted to an amorphous oxide shell, results in physical deformation of the InAs core, demonstrating the mechanical compliance of these ultrathin NWs. We note that since the ultrathin NWs grown using this method lack site control due to the randomness of the atomic Au diffusion path, external alignment will be necessary to realize array-based devices using such NWs. This is the first report on high quality 5 nm diameter InAs NWs with abrupt radial heterojunctions. Core/shell NWs with less lattice mismatch between the core and the shell will be grown in the future to study the possibility of completely dislocation-free core/shell heterostructures as well as investigations on electronic device applications.

Acknowledgements

This work was supported by the Office of Naval Research Young Investigator Program Award N000141110634 (KJ and XL) and NSF DMR award #1006581 (PKM).

Notes and references

Department of Electrical and Computer Engineering, Micro and Nanotechnology Laboratory, University of Illinois at Urbana-Champaign, Urbana, Illinois, 61801

†Corresponding Author. Email: xiuling@illinois.edu

Electronic Supplementary Information (ESI) available: [SEM images of bimodal NW growth using various size Au colloids, SEM image of 3μm long ultrathin InAs NW, SEM image showing proximity effect, EDX composition analysis of the tip of an ultrathin InAs NW, SEM image showing effect of temperature hold prior to NW growth, SEM image showing NW tip after extended growth, HRTEM image showing NW

sidewall of 50nm InAs NW, SEM image showing early stage of Au atom spreading process].

1 http://public.itrs.net, *International Technology Roadmap for Semiconductors*, 2012.
2 D. J. Frank, R. H. Dennard, E. Nowak, P. M. Solomon, Y. Taur, and H. S. P. Wong, *Proceedings of the IEEE* 2001, **89**, 259.
3 H. Wakabayashi, S. Yamagami, N. Ikezawa, A. Ogura, M. Narihiro, K. I. Arai, Y. Ochiai, K. Takeuchi, T. Yamamoto, and T. Mogami, *IEDM* 2003, 20.7.1.
4 D. Hisamoto, W. C. Lee, J. Kedzierski, H. Takeuchi, K. Asano, C. Kuo, E. Anderson, T. J. King, J. Bokor, and C. Hu, *IEEE Trans. Electron Devices* 2000, **47**, 2320.
5 H. S. P. Wong, D. J. Frank, and P. M. Solomon, *IEDM* 1998, 407.
6 H. T. Ng, J. Han, T. Yamada, P. Nguyen, Y. P. Chen, and M. Meyyappan, *Nano Lett.* 2004, **4**, 1247.
7 J. P. Colinge, C. W. Lee, A. Afzalian, N. D. Akhavan, R. Yan, I. Ferain, P. Razavi, B. O'Neill, A. Blake, M. White, A. M. Kelleher, B. McCarthy and R. Murphy, *Nature Nanotech.* 2010, **5**, 225.
8 R. H. Yan, A. Ourmazd, K. F. Lee, and D. Y. Jeon, *Appl. Phys. Lett.* 1991, **59**, 3315.
9 J. Knoch, W. Riess, and J. Appenzeller, *IEEE Electron Device Lett.* 2008, **29**, 372.
10 M. A. Khayer, and R. K. Lake, *J. Appl. Phys.* 2010, **107**, 014502.
11 V. G. Dubrovskii, N. V. Sibirev, G. E. Cirlin, I. P. Soshnikov, W. H. Chen, R. Larde, E. Cadel, P. Pareige, T. Xu, B. Grandidier, J. P. Nys, D. Stievenard, M. Moewe, L. C. Chuang, and C. Chang-Hasnain, Phys. Rev. B. 2009, **79**, 205316.
12 L. E. Fröberg, W. Seifert, and J. Johansson, Phys. Rev. B. 2007, **76**, 153401.
13 G. Shen, B. Liang, X. Wang, H. Huang, D. Chen, and Z. L. Wang, *ACS Nano* 2011, **5**, 6148.
14 X. Wang, G. Wang, P. Slattery, J. Z. Zhang, and Y. Li, *Cryst. Growth Des.* 2010, **10**, 2479.
15 X. Duan, J. Wang, and C. M. Lieber, *Appl. Phys. Lett.* 2000, **76**, 1116.
16 A. Razavieh, D. B. Janes, and J. Appenzeller, IEEE Trans. Electron Devices 2013, **60**, 2071.
17 S. A. Dayeh, D. P. R. Aplin, X. Zhou, P. K. L. Yu, E. T. Yu, and D. Wang, *Small* 2007, **3**, 326.
18 S. A. Fortuna, J. Wen, I. S. Chun and X. Li, Nano Lett. 2008, 8, 4421.
19 A. Mikkelsen, N. Skold, L. Ouattara and E. Lundgren, *Nanotechnology* 2006, **17**, S362.
20 R. S. Dowdy, D. A. Walko and X. Li, *Nanotechnology* 2013, **24**, 035304.
21 S. A. Fortuna and X. Li, *Semicond. Sci. Technol.* 2013, **25**, 024005.
22 S. A. Dayeh, E. T. Yu and D. Wang, *Nano Lett.* 2007, **7**, 2486.
23 B. Mandl, J. Stangl, T. Martensson, A. Mikkelsen, J. Eriksson, L. S. Karlsson, G. Bauer, L. Samuelson and W. Seifert, *Nano Lett.* 2006, **6**, 1817.
24 E. Dailey and J. Drucker, *J. Appl. Phys.* 2009, **105**, 064317.
25 M. I. den Hertog, J. L. Rouviere, F. Dhalluin, P. J. Desre, P. Gentile, P. Ferret, F. Oehler and T. Baron, *Nano Lett.* 2008, **8**, 1544.
26 P. Madras, E. Dailey and J. Drucker, *Nano Lett.* 2010, **10**, 1759.
27 J. B. Hannon, S. Kodambaka, F. M. Ross and R. M. Tromp, *Nature* 2006, **440**, 69.
28 R. Novakovic, E. Ricci and F. Gnecco, *Surface Science* 2006, **600**, 5051.
29 K. A. Dick, K. Deppert, L. S. Karlsson, L. R. Wallenberg, L. Samuelson and W. Seifert, *Adv. Funct. Mater.* 2005, **15**, 1603.
30 H. Heslot, N. Fraysse, and A. M. Cazabat, *Nature*, 1989, **338**, 640.
31 S. A. Dayeh, E. T. Yu and D. Wang, *Small* 2007, **3**, 1683.
32 S. Raychaudhuri and E. T. Yu, *J. Appl. Phys.* 2006, **99**, 114308.
33 S. Raychaudhuri and E. T. Yu, *J. Vac. Sci. Technol. B* 2006, **24**, 2053.
34 R. Popovitz-Biro, A. Kretinin, P. Von Huth and H. Shtrikman, *Cryst. Growth Des.* 2011, **11**, 3858.
35 S. A. Dayeh, W. Tang, F. Boioli, K. L. Kavanagh, H. Zheng, J. Wang, N. H., Mack, G. Swadener, J. Y. Huang, L. Miglio, K. N. Tu and S. T. Picraux, *Nano Lett.* 2013, **13**, 1869.